JOURNAL OF MATERIALS SCIENCE **40** (2005) 2959–2964

$M_{23}C_6$ precipitation behavior in a Ni-base superalloy M963

L. Z. HE*,†, Q. ZHENG, X. F. SUN, G. C. HOU, H. R. GUAN, Z. Q. HU
Department of Superalloys, Institute of Metal research, Chinese Academy of Science, 72 Wenhua Road, Shenyang 110016, People's Republic of China
E-mail: cybhlz@163.net

The $M_{23}C_6$ precipitation behavior in a cast Ni-base superalloy M963 was investigated after tensile creep testing at 800°C and strain-controlled low cycle fatigue testing at 700–950°C. During high temperature creep and low cycle fatigue, the primary MC decomposed into M_6C continuously, and a great amount of secondary carbide, chromium-rich $M_{23}C_6$, precipitated preferentially in the periphery of MC and $\gamma + \gamma'$ eutectic at grain boundaries. $M_{23}C_6$ was rarely present in grain interior, indicating that grain boundary promoted $M_{23}C_6$ carbide precipitation. The $M_{23}C_6$ precipitation was closely dependent on the stress state and testing temperature, seemed to be independent of the total strain amplitude. $M_{23}C_6$ is unstable during low cycle fatigue testing. The occurrence of $M_{23}C_6$ precipitation was sharply reduced during low cycle fatigue testing at 950°C. Crack was easily initiated at interface between MC and matrix, while fine $M_{23}C_6$ was effective to prevent grain boundary migration.

1. Introduction

The influence of grain boundary precipitates (for example, $M_{23}C_6$) on the properties of Ni-base superalloys has been recognized [1–4]. MC precipitation reactions also influence the properties of superalloys [5, 6]. Recently, numerous investigations have been characterized the formation sequence, composition and morphological evolution of MC, from slow to rapid solidification conditions [7–10]. Hf and Mg addition can significantly modify the MC morphology, and enhance the creep and fatigue properties of superalloys at elevated temperatures [11–14]. Extensive studies have been shown that prolonged thermal and stress exposures can overage the alloy microstructure, that is, γ' phase coalescence, formation of continuous secondary $M_{23}C_6$ films on the grain boundary, primary MC degeneration and σ phase formation [15–17]. Unfortunately, up to date, limited information is available for $M_{23}C_6$ precipitation behavior during creep and strain controlled low cycle fatigue tests. M963, a γ' and carbide strengthened cast Ni-base superalloy, is being used in aircraft turbine engines and other high temperature structural components. The present work is aimed to investigate the effect of stress and temperature on $M_{23}C_6$ precipitation mechanism during creep testing at 800°C and low cycle fatigue testing at 700–950°C in this alloy.

2. Experimental

The chemical composition of M963 master superalloy used in this work is as follows (in wt.%): 0.15C, 9Cr, 10Co, 11W, 1.5Mo, 5.6Al, 1.0Nb, 2.5Ti, and balance Ni. The master alloy was remelted in a VIM25F vacuum induction furnace, superheated to 1600°C for 5 min till completely melted [18], then cast into test bars. The solution treatment was performed at 1210°C for 4 h, and followed by air cooling. Then the solution treated bars were machined into specimens for creep test with a diameter of 8 mm and a gauge length of 50 mm and for low cycle fatigue test with a diameter of 5 mm and a gauge length of 25 mm. All test specimens were ground along the gage length in the longitudinal direction with SiC paper down to grit 1200 in order to minimize the influence of surface defects on test results. Before testing, nondestructive evaluation was used to check out the casting micropores in the test bars.

Constant load tensile creep tests were performed in air at 560 MPa stress and 800°C. The temperature was measured by two or three thermocouples attaching to the gage length part of specimen, and was controlled within ±2°C. The inductive transducers could detect strain variations as small as 5×10^{-4} and were continuously recorded.

A servohydraulic testing machine was used to carry out the fatigue tests at 700–950°C in air. The total axial strain was measured and controlled by an extensometer mounted upon the ledges of specimens. The total strain amplitude varied from ±0.15% to ±0.6% with a fully reversed strain-controlled push-pull mode, i.e., $R = -1$. The strain rate was 4×10^{-3} s^{-1}, applied in a triangular waveform. The temperature fluctuation over

*Author to whom all correspondence should be addressed.
†*Present address*: 6/24 Vickery St. Gwynneville, NSW 2500, Australia.

the gage length area was maintained within ±2°C. All specimens were run to failure. Three specimens were prepared for every strain range.

A JSM-6301F field emission scanning electron microscope (SEM) equipped with energy dispersive analytical X-ray (EDAX) was used to observe the microstructure characteristics. SEM specimens were prepared with longitudinal sections of fracture surface from creep and low cycle fatigue testing bars and were etched chemically in a solution of 40 ml C_2H_5OH + 1.5 g $CuSO_4$ + 20 ml H_2O. High magnification observation was carried out using a Philip EM420 transmission electron microscope (TEM). The TEM foil was prepared by twin-jet thinning electrolytically in a solution of 7 vol.% perchloric acid in alcohol at −30°C.

3. Results

3.1. Initial microstructures

Fig. 1a shows the typical as-cast microstructure of the alloy, which contains γ matrix, γ' precipitate, $\gamma + \gamma'$ eutectic and primary carbide. X-Ray diffraction analysis (XRD) (Fig. 3a) and EDAX analysis only find MC carbide in the as-cast alloy. The MC carbide is rich in Ti and Nb elements (Fig. 1b), with the composition of (wt.%) Ti 43.12, Cr 1.96, Ni 7.53, Nb 23.96, Mo 4.52, W 18.08. It can be seen that the MC carbide is present as a discrete blocky morphology at grain boundary, and a well-distributed Chinese-script morphology at interdendritic region, such a carbide characteristic of the as-cast alloy is similar to that of Mar-M247 alloy [19]. Yin etc. have reported that superheated treatment can change the primary carbide morphology from a blocky appearance to a more fine and homogeneously distributed Chinese-script morphology [18]. During solution treatment, MC carbide decompose into M_6C carbides by the reaction of $MC + \gamma \rightarrow M_6C + \gamma'$ (Fig. 2a). At the same time, MC carbide is still intact as primary form. EDAX analysis shows that M_6C carbide is rich in W and Mo elements (Fig. 2b), has the composition of (wt.%) Al 0.49, Ti 1.23, Cr 6.58, Co 5.41, Ni 14.93, Nb 2.45, Mo 6.96, W 61.95. XRD (Fig. 3) and EDAX analysis can not find any trace of $M_{23}C_6$ carbide in as-cast or solution-treated alloy. However, many researches have reported that profuse $M_{23}C_6$ carbide particles precipitate both at grain boundary and grain interior during solidification and heat treatment processes [20–23]. In this work, no $M_{23}C_6$ are observed in the microstructures of as-cast and solution-treated alloy, it is due to the relative high Cr content and low W and Mo contents in their used materials.

3.2. Microstructures after creep and low cycle fatigue

Fig. 4 shows the microstructures after creep test for 40 h to a strain of 0.5% at 800°C under a constant tensile stress of 560 MPa. It can be seen that a profusion of secondary precipitates have been produced. During creep testing, MC continuously decomposes

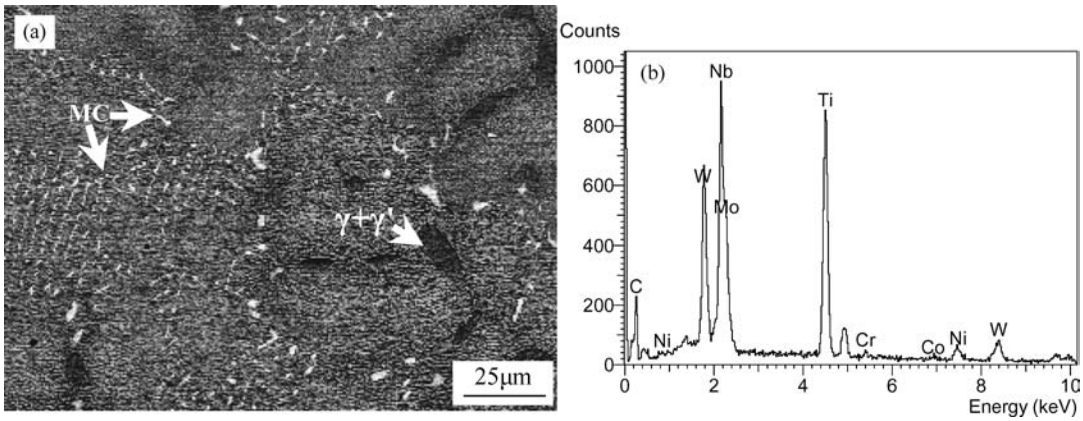

Figure 1 (a) Backscattered electron image of as-cast alloy in transverse cross section and (b) EDAX of MC.

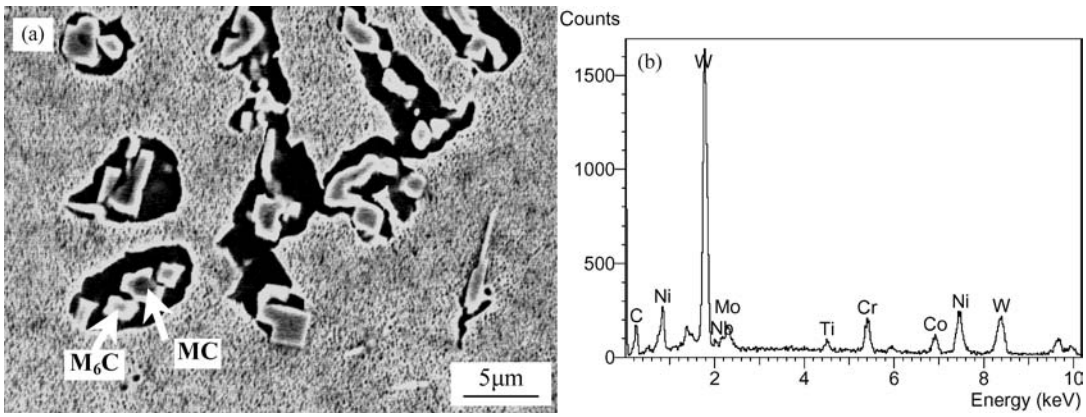

Figure 2 (a) Second electron image of solution treated alloy in transverse cross section and (b) EDS of M_6C.

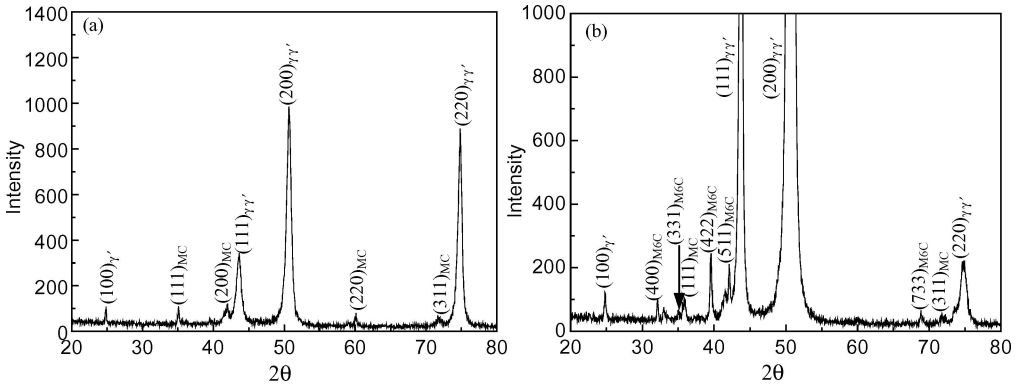

Figure 3 Results of XRD analysis of M963 alloy. (a) as-cast, (b) solution treated.

into M_6C (Fig. 4a and b), the transformed M_6C has irregular shape. There is a dense distribution of fine precipitates with cuboidal shape at dendritic core regions (Fig. 4c). The electron diffraction analysis (Fig. 4d) demonstrates that all these precipitates are M_6C. At grain boundary (Fig. 4e), lots of extremely fine particles preferentially precipitate on the surface of $\gamma + \gamma'$ eutectic. EDAX analysis (Fig. 4f) indicates that the carbide is chromium-rich. TEM image (Fig. 4g) shows that the grain boundary precipitates are only about 50 nm and have irregular shape. The electron diffraction analysis (Fig. 4h) indicates that the grain boundary precipitates are $M_{23}C_6$. It is also found that the $M_{23}C_6$ is mainly present at grain boundary, rarely at grain interior and interdendritic regions.

Fig. 5 shows the microstructures after low cycle fatigue testing to fracture at 700–950°C. It can be seen that only MC and M_6C and still no $M_{23}C_6$ are observed after low cycle fatigue at 700°C, $\Delta\varepsilon_t/2 = 0.25\%$, 60 h and at 800°C, $\Delta\varepsilon_t/2 = 0.23\%$, $t = 74$ h (Fig. 5a and b). After low cycle fatigue at 900°C, $\Delta\varepsilon_t/2 = 0.25\%$, $t = 9$ h (Fig. 5c), some extremely fine $M_{23}C_6$ particles start to be found at the edge of grain boundary MC carbide (marked by arrow), and still are absent at grain interior and interdendritic regions. It can be noted that MC decomposition results in a considerable reduction in size. When low cycle fatigue testing at 950°C, the occurrence of grain boundary $M_{23}C_6$ is sharply shortened to be at $\Delta\varepsilon_t/2 = 0.5\%$, $t = 8$ min (Fig. 5d). With the increment of exposure time ($\Delta\varepsilon_t/2 = 0.15\%$, $t = 93$ h), the number and the size of grain boundary $M_{23}C_6$ increase (Fig. 5e). The backscattered electron image also shows the contrast between the carbides, the brighter one is M_6C carbide, the gray one is MC, and the darker one which contrast is close to that of the matrix is $M_{23}C_6$. The line scanning analysis of MC in Fig. 5e shows that a substantial change of MC constituent element concentration toward its edges (it is known that the element concentration of MC carbide can vary in a wide range), a tendency of Ti, Nb and W contents decrease from the center to the periphery is evident, but Cr content increases, the EDAX analysis from A to D constituents are also listed in Table I. It can be seen that the matrix (marked by A) contains high Ni, W, Cr and Ti contents, and B and C constituents contain more Nb, Ti, and W contents but lower Cr content than matrix, indicates that B and C constituents are still MC due to high Nb and Ti contents. While D constituent contains more Cr and lower W contents than B and C constituents, indicates that it is the $M_{23}C_6$. These phenomena indicate that the process of MC decomposition accompanies the change of MC composition. The reaction of M_6C decomposition into $M_{23}C_6$ can not be found under all testing conditions.

TABLE I EDS results for compositions of the positions marked in Fig. 5e after low cycle fatigue (wt%)

	Al	Ti	Cr	Co	Nb	Mo	W	Ni
A	3.29	8.2	10.48	7.13	2.81	0.8	17.88	49.4
B	0.77	21.29	4.83	3.25	23.78	2.29	24.86	18.93
C	0.3	27.9	1.2	–	32.68	4.99	29.34	3.6
D	3.19	2.05	29.81	5.75	5.0	4.09	16.39	33.72

4. Discussion

4.1. Kinetics for Grain boundary $M_{23}C_6$ carbide precipitation

EDAX analysis indicates that the composition of primary MC in M963 alloy contains Ti, Nb, W, Mo, Ni and Cr. The replacement of the strong carbide forming atoms such as Ti and Nb with Mo, Ni and Cr atoms is known to weaken the interatomic bonds in the MC resulting in a decrease of their stability [24]. This leads to the MC decomposition into more stable $M_{23}C_6$. The EDAX analysis result shows that a substantial change of the MC carbide element concentration toward its edges, which indicates that a tendency of carbon content decreases from the center to the edges of MC.

Apparently, diffusion of carbon from the metastable MC into surrounding γ matrix takes place during high temperature low cycle fatigue testing, creating a favorable condition for the formation of more stable lower order $M_{23}C_6$ on the MC/γ interface. The MC serves as a carbon source and γ matrix as a chromium reservoir for the formation of chromium-rich $M_{23}C_6$ [24]. It should be noted that the $M_{23}C_6$ mainly locates at or near the grain boundaries, which demonstrates that the abundance of the grain-boundary diffusion assists the process of MC decomposition than that in grain interiors. The much finer grain boundary $M_{23}C_6$ will effectively prevent grain boundary migration during deformation, strengthening grain boundary, and be beneficial to the fatigue property of the alloy.

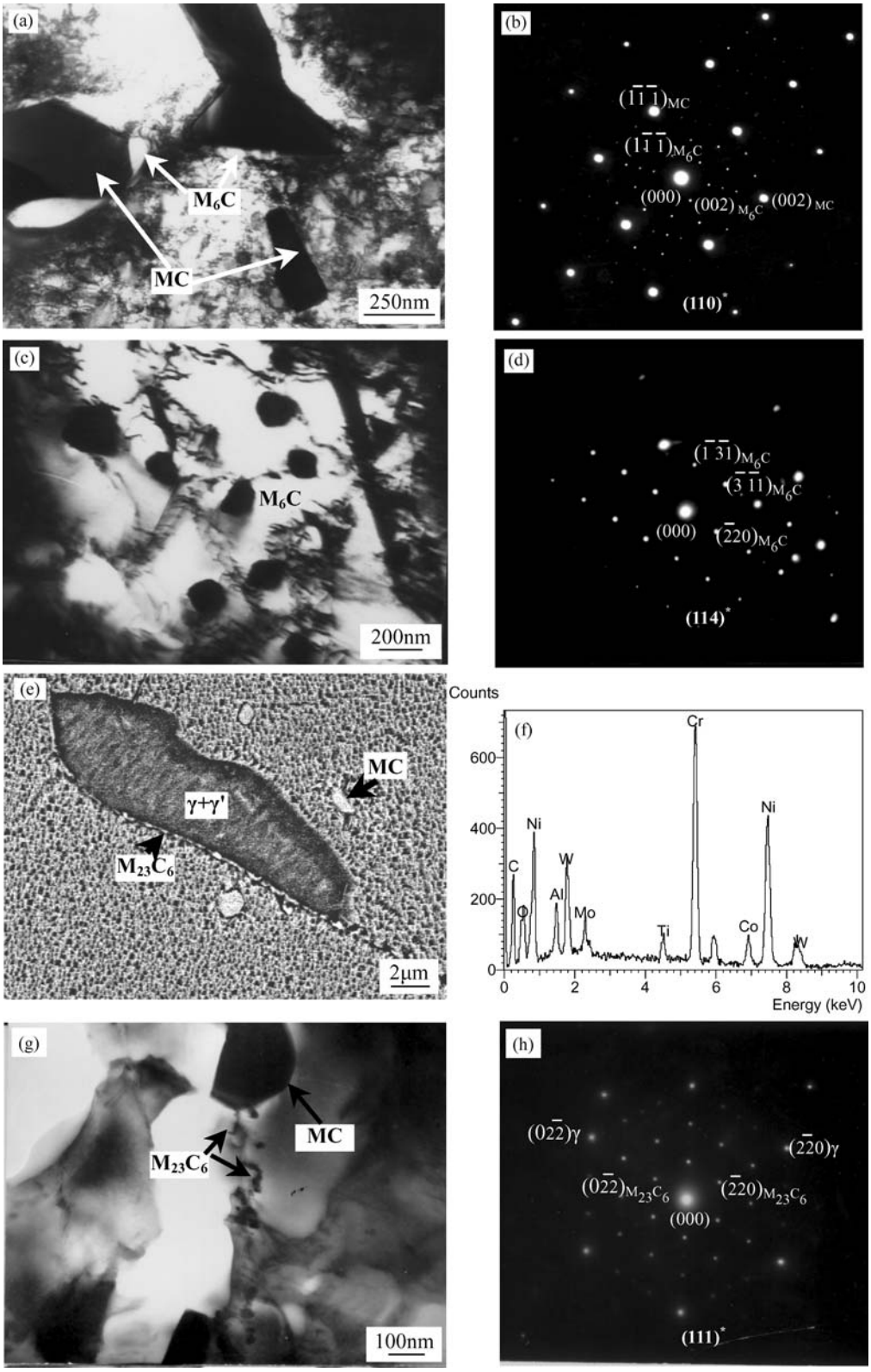

Figure 4 Microstructures after creep tested for 40 h to a strain of 0.5% at 800°C under tensile stress of 560 MPa. (a) TEM image showing transformed M_6C, (b) diffraction pattern of transformed M_6C, (c) TEM image showing precipitated M_6C, (d) diffraction pattern of precipitated M_6C, (e) SEM image showing $M_{23}C_6$, (f) EDS of $M_{23}C_6$, (g) TEM image showing $M_{23}C_6$, and (h) diffraction pattern of $M_{23}C_6$.

4.2. Effect of stress state and temperature on $M_{23}C_6$ precipitation

According to the results of this work, it can be seen that the $M_{23}C_6$ precipitation is closely dependent on the stress state and temperature, and seems to be independent of the total strain amplitude. Under tensile creep testing, $M_{23}C_6$ is observed at 800°C, $t = 39$ h. But under a fully reversed strain-controlled push-pull mode of low cycle fatigue testing, $M_{23}C_6$ can not be observed even at 800°C, $t = 74$ h, and is found at 900°C, $t = 9$ h. The occurrence of $M_{23}C_6$ is sharply shortened to 8 min at 950°C. Xu *et al*. [25] reported that $M_{23}C_6$ precipitates in Udimet 520 alloy over a wide range of aging temperatures varying between 600 and 1050°C, the start of grain boundary $M_{23}C_6$ precipitation was only 80 s at 800°C, and the precipitating peak was

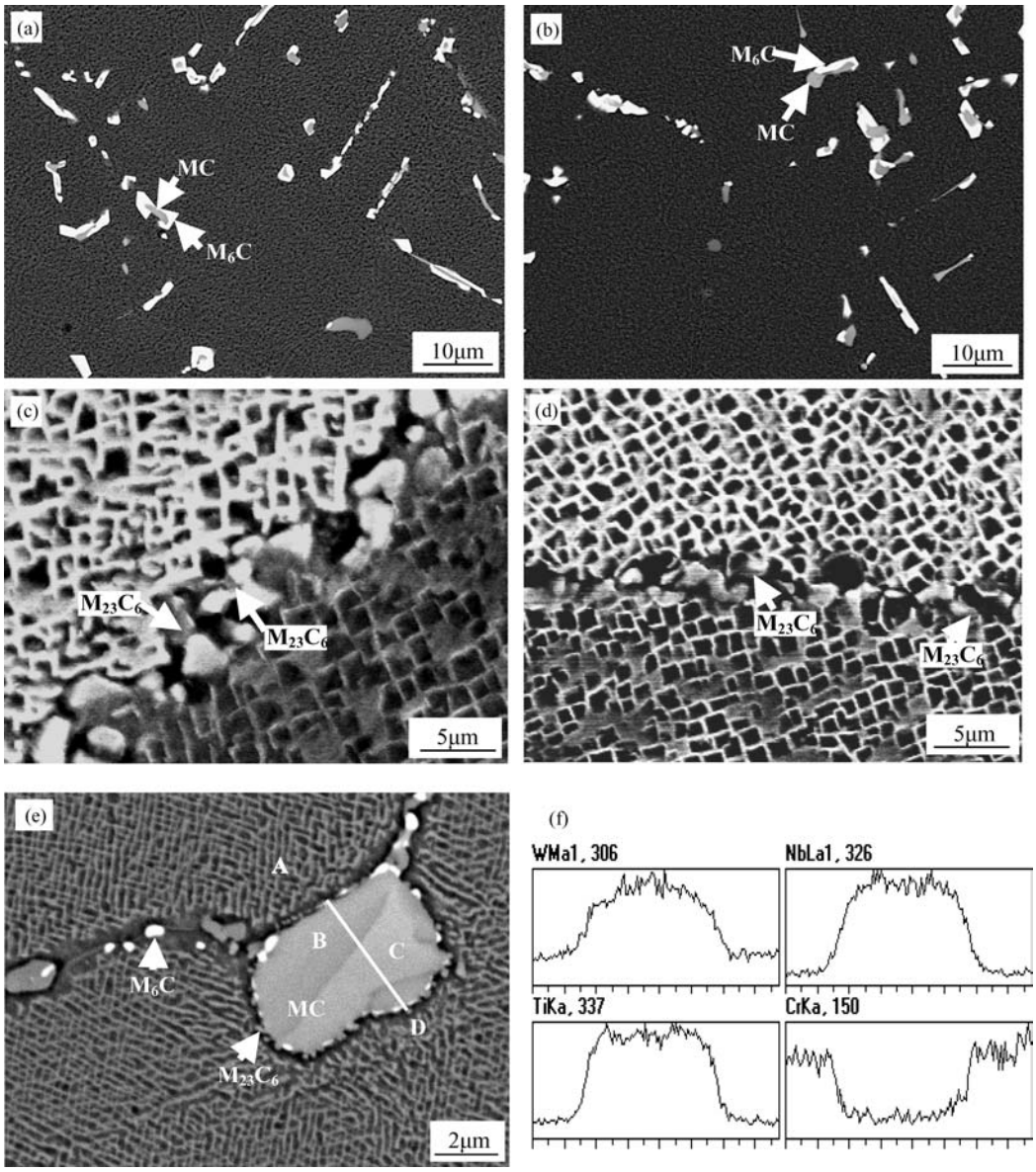

Figure 5 (a) BSD image showing microstructures at 700°C, $\Delta\varepsilon_t/2 = 0.25\%$, 60 h, (b) BSD image showing microstructure at 800°C, $\Delta\varepsilon_t/2 = 0.23\%$, 74 h, (c) SEI image showing microstructure at 900°C, $\Delta\varepsilon_t/2 = 0.25\%$, 9 h, (d) SEI image showing microstructure at 950°C, $\Delta\varepsilon_t/2 = 0.5\%$, 8 min, (e) BSD image showing microstructure at 950°C, $\Delta\varepsilon_t/2 = 0.15\%$, 93 h, (f) line scanning of carbide marked in (e).

between 760 and 1050°C. From the results of this work, it can be deduced that the tensile stress is likely to accelerate $M_{23}C_6$ precipitation, and the precipitating peak of $M_{23}C_6$ during low cycle fatigue testing is at 950°C, the prolonged exposure time only results in the $M_{23}C_6$ growth. When low cycle fatigue testing at 950°C, it can also be found that the size of $M_{23}C_6$ change from 200 nm ($\Delta\varepsilon_t/2 = 0.5\%$, $t = 8$ min) to 800 nm ($\Delta\varepsilon_t/2 = 0.15\%$, $t = 93$ h), this indicates that $M_{23}C_6$ is unstable under push-pull stress state. Mino *et al.* [26] reported the grain boundary migration during creep at 1000°C in Inconel 617 alloy. Kihara *et al.* [27] observed that grain boundary carbides migrated from grain boundaries that were under compressive stress to grain boundaries that are under tensile stress. This was due to the dissolution of relatively unstable carbides on the compressive boundaries, the diffusion of the solute atoms to the tensile boundaries and reprecipitation of the carbides at the tensile boundaries. The rate of grain boundary carbide migration depended on grain size, i.e., the larger the grain size, the longer the time for carbide to reach the tensile boundaries. Carbide migration can not be observed in this work due to much larger grain size.

4.3. Effect of grain boundary $M_{23}C_6$ carbide during deformation

The effect of carbide on properties is contradictory, strengthening grain and interdendritic boundaries, retarding boundary migration, pinning dislocation, hardening the matrix. On the other hand, their interface with the matrix becomes the initiation sites for fracture [28]. In this work, EDS analysis at selected locations on the fracture surface shows the presence of lots of carbide particles. The carbides are qualitatively determined to be MC and M_6C and found to be situated at the grain boundaries as well as in the matrix. Coarse carbide particles dispersed in the matrix can be postulated to initiate microvoids at their interface with matrix, which would lead to dimples in the ductile fracture process

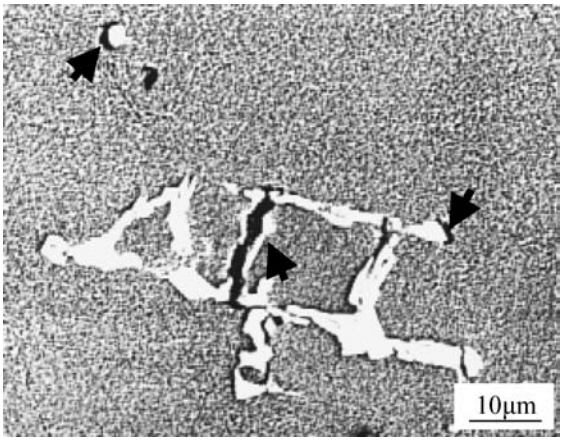

Figure 6 Effect of MC during deformation after low cycle fatigue at 900°C, $\Delta\varepsilon_t/2 = 0.6\%$, 5 min.

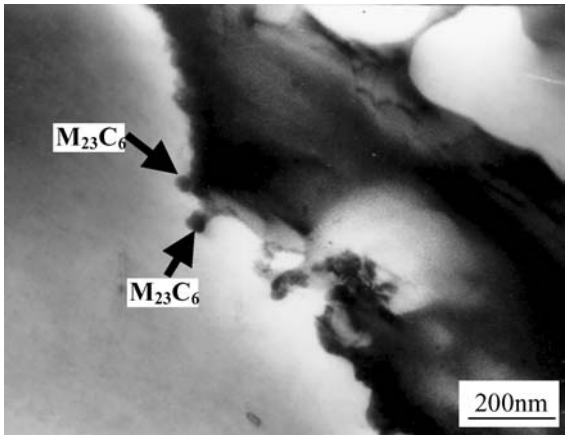

Figure 7 Effect of $M_{23}C_6$ during deformation after low cycle fatigue at 950°C, $\Delta\varepsilon_t/2 = 0.2\%$, 7 h.

of the matrix. It also can be observed that the carbides themselves crack during low cycle fatigue (Fig. 6). During high temperature creep and low cycle fatigue tests, coarse primary MC carbide sluggishly decomposes into extremely fine $M_{23}C_6$ carbide at grain boundary, which can strengthen grain boundary and prevent grain boundary migration during deformation (Fig. 7).

5. Conclusion

During creep and low cycle fatigue tests, the primary MC decomposes sluggishly and a profusion of second carbide, chromium-rich $M_{23}C_6$ precipitates dominantly at grain boundary.

$M_{23}C_6$ precipitation is highly dependent on the stress state and testing temperature, irrelative with total strain amplitude of low cycle fatigue.

The $M_{23}C_6$ precipitation peak is 950°C during low cycle fatigue.

Fine $M_{23}C_6$ can effectively prevent grain boundary migration and strengthen grain boundary.

References

1. A. K. KOUL and W. WALLACE, *Metall. Trans.* A **13** (1982) 673.
2. J. M. LARSON and S. FLOREEN, *ibid.* **8** (1977) 51.
3. T. M. ANGELIU and G. S. WAS, *ibid.* **21** (1990) 2097.
4. P. E. LI, J. S. ZHANG and J. Z. JIN, *ibid.* **23** (1992) 1379.
5. A. MITCHELL, S. L. COCKCROFT, C. E. SCHVEZOV, A. J. SCHMALZ, J. N. LOQUET and J. FERNIHOUGH, *High Temp. Mater. Process* **15**(1/2) (1996) 27.
6. M. C. PANDEY, D. V. V. SATYANARAYANA and D. M. R. TAPLIN, *Mater. Sci. Technol.* **10**(11) (1994) 936.
7. J. CHEN, J. H. LEE, C. Y. JO, S. J. CHOE and Y. T. LEE, *Mater. Sci. Eng. A* **247** (1998) 113.
8. W. R. SUN, J. H. LEE, S. M. SEO, S. J. CHOE and Z. Q. HU, *ibid. 271* (1999) 143.
9. H. M. WANG, L. G. YU, X. X. LI and D. JIANG, *Sci. Technol. Adv. Mater.* **2** (2001) 173.
10. Q. Z. CHEN, C. N. JONES and D. M. KNOWLES, *Scr. Mater.* **47** (2002) 669.
11. M. J. STARINK, H. CAMA and R. C. THOMSON, *ibid.* **38**(1) (1998) 73.
12. Q. Z. CHEN, C. N. JONES and D. M. KNOWLES, *Acta Mater.* **50** (2002) 1095.
13. H. Y. BOR, C. G. CHAO and C. Y. MA, *Scr. Mater.* **38**(2) (1998) 329.
14. R. V. MINER, *Metall. Trans. A* **8** (1977) 259.
15. R. A. STEVENS and P. E. J. FLEWITT, *J. Mater. Sci.* **13** (1978) 367.
16. *Idem.*, *Mater. Sci. Eng.* **37** (1979) 237.
17. X. B. HUANG, Y. KANG, H. H. ZHOU, Y. ZHANG and Z. Q. HU, *Mater. Lett.* **36** (1998) 210.
18. F. S. YIN, X. F. SUN, J. G. LI, H. R. GUAN and Z. Q. HU, *Scripta Mater.* **48**(4) (2003) 425.
19. J. CHEN, J. H. LEE, C. Y. JO, S. J. CHOE and Y. T. LEE, *Mater. Sci. Eng. A* **427** (1998) 113.
20. H. E. COLLINS, *Metall. Trans.* **5**(1) (1974) 189.
21. W. L. MANKINS, J. C. HOSIER and T. H. BASSFORD, *ibid.* **5** (1974) 2579.
22. T. TAKAHASHI, J. FUJIWARA, T. MATSUSHIMA, M. KIYOKAWA, I. MORIMOTO and T. WATANABE, *Trans. Iron Steel Inst. Jpn.* **18** (1978) 221.
23. G. S. WAS and V. B. RAJAN, *Metall. Trans. A* **18** (1987) 1313.
24. E. W. ROSS and C. T. SIMS, in "Superalloys II," edited by C. T. Sims, N. S. Stoloff and W. C. Hagel (New York, 1984), Chap. 4.
25. S. XU, J. I. DICKSON and A. K. KOUL, *Metall. Mater. Trans. A* **29** (1998) 2687.
26. K. MINO and A. OHTOMO, *Trans. Iron Steel Inst. Jpn.* **18** (1978) 731.
27. S. KIHARA, J. B. NEWKIRK, A. OHTOMO and Y. SAIGA, *Metall. Trans. A* **11** (1980) 1019.
28. G. A. RAO, M. KUMAR, M. SRINIVAS and D. S. SARMA, *Mater. Sci. Eng. A* **355** 2003 114.

Received 26 January
and accepted 19 October 2004